

**GA-A22337**

**INITIAL OPERATION OF  
THE DIVERTOR THOMSON SCATTERING  
DIAGNOSTIC ON DIII-D**

by  
**T.N. CARLSTROM, C.L. HSIEH, R.E. STOCKDALE,  
D.G. NILSON, and D.N. HILL**

**MAY 1996**

**GA-A22337**

**INITIAL OPERATION OF  
THE DIVERTOR THOMSON SCATTERING  
DIAGNOSTIC ON DIII-D**

by  
**T.N. CARLSTROM, C.L. HSIEH, R.E. STOCKDALE,  
D.G. NILSON,\* and D.N. HILL\***

This is a preprint of a paper to be presented at the  
11th Topical High Temperature Plasma Diagnostics  
Conference, May 12-16, 1996, in Monterey,  
California, and to be published in *Rev. Sci. Instrum.*

\*Lawrence Livermore National Laboratory, Livermore, California.

**Work supported by  
the U.S. Department of Energy  
under Contract Nos. DE-AC03-89ER51114  
and W-74095-ENG**

**GA PROJECT 3466  
MAY 1996**

## ABSTRACT

The first Thomson scattering measurements of  $n_e$  and  $T_e$  in the divertor region of a tokamak are reported. These data are used as input to boundary physics codes such as UEDGE and DEGAS and to benchmark the predictive capabilities of these codes. These measurements have also contributed to the characterization of tokamak disruptions. A Nd:YAG laser (20 Hz, 1 J, 15 ns, 1064 nm) is directed vertically through the lower divertor region of the DIII-D tokamak. A custom, aspherical collection lens ( $f/6.8$ ) images the laser beam from 1–21 cm above the target plates into eight spatial channels with 1.5 cm vertical and 0.3 cm radial resolution. 2D mapping of the divertor region is achieved by sweeping the divertor X-point location radially through the fixed laser beam location. Fiber optics carry the light to polychromators whose interference filters have been optimized for low  $T_e$  measurements. Silicon avalanche photo diodes measure both the scattered and plasma background light. Temperatures and densities are typically in the range of 5–200 eV and  $1-10 \times 10^{19} \text{ m}^{-3}$  respectively. Low temperatures,  $T_e < 1 \text{ eV}$ , and high densities,  $n_e > 8 \times 10^{20} \text{ m}^{-3}$  have been observed in detached plasmas. Background light levels have not been a significant problem. Reduction of the laser stray light permits Rayleigh calibration. Because of access difficulties, no in-vessel vacuum alignment target could be used. Instead, an *in situ* laser alignment monitor provides alignment information for each laser pulse. Results are compared with Langmuir

probe measurements where good agreement is found except for regions of high  $n_e$  and low  $T_e$  as measured by Thomson scattering.

## INTRODUCTION

In this paper we describe the commissioning (summer, 1995) of the Divertor Thomson Scattering (DTS) System for the DIII-D tokamak, which has been used to measure the complete two-dimensional density and temperature profiles in the tokamak divertor plasma below the X-point for the first time. This work is motivated by the need to reduce the expected scrape-off layer energy and particle transport to the divertor target plates by more than an order of magnitude in future high power tokamaks such as the proposed ITER device. The most likely means for achieving this will be to seed the divertor with impurities in order to increase the local radiative losses. Our measurements are significant because they document for the first time in these highly radiating plasmas how  $n_e$  and  $T_e$  vary on magnetic flux surfaces in the divertor with sufficient spatial resolution to allow comparison with theoretical predictions of heat and particle transport.

In the remainder of this paper we discuss the design of the system, important features unique to the low temperatures found in the divertor, calibration, and test results. Finally, we show typical density and temperature data from a divertor plasma in which deuterium gas injection was used to raise the divertor neutral pressure and radiative losses to the point where almost all the power flowing in the SOL is lost via atomic processes such as radiation and charge exchange. In this case, we find very low temperatures (below 2 eV) throughout the divertor region, a

sharp drop in electron plasma pressure along flux surfaces, and a radial shift in the peak of the density profile.

## II. SYSTEM DESCRIPTION

This system is an extension of the pre-existing 8 laser, multipulse Thomson scattering diagnostic previously reported.<sup>1</sup> A brief description of the system is given here for completeness. Further details of the divertor Thomson scattering system design are given in Ref. 2. One of the 8, Nd:YAG lasers (20 Hz, 1 J, 15 ns, 1064 nm) is redirected from the core plasma to the divertor plasma with mirrors on an optics table located beneath the DIII-D vessel as shown in Fig. 1. The 5.6 m focal length lens with a 20 mm aperture focuses the beam through a series of 12 light baffles and produces a 3.5 mm diameter spot in the scattering region. A 3 mm radial clearance is maintained between the beam and the baffle cones in the vertical entrance port. At the top of the vessel, the laser beam passes through six large aperture baffles (39 mm dia.), an exit vacuum window tilted at Brewster's angle, a beamsplitter for an alignment camera, and finally a beam dump constructed of NG-4 glass. A Glan-Laser polarizer is used to improve the polarization characteristics of the laser beam and reduce the stray light reflecting from the exit window. Additional techniques and methods used to reduce the stray light level are given in a companion paper at this conference.<sup>3</sup>

A two-element  $f/6.8$  collection lens images the 20 cm vertical scattering region onto 12 rectangular fiber arrays (1.5 mm  $\times$  3.0 mm) with a system demagnification of 0.29. The lens structure and fiber arrays

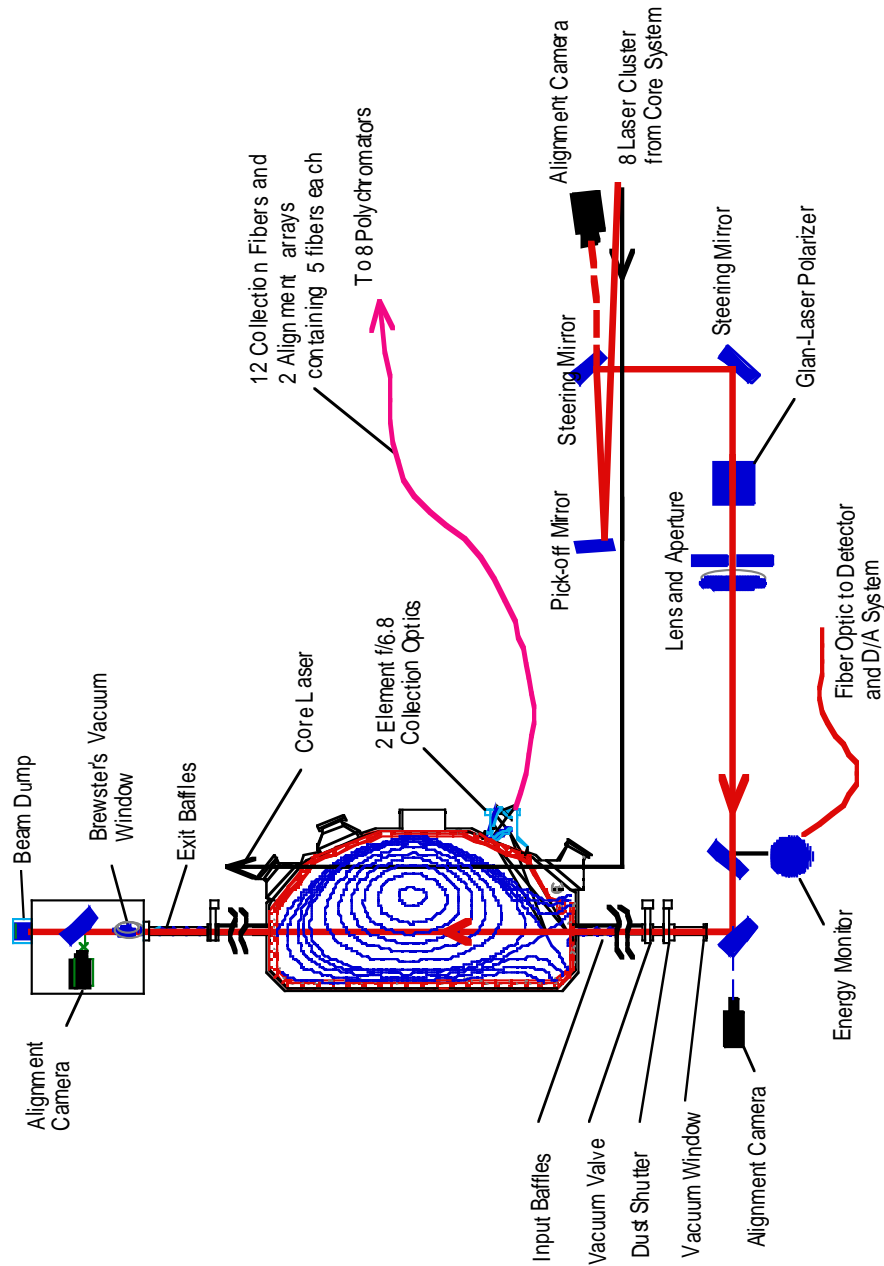


Fig. 1. Schematic layout of the divertor Thomson scattering diagnostic showing the laser beam propagation on the input optics table, through the vacuum window, baffles, and DIII-D vessel, and exiting from the vessel into a beam dump. Also illustrated are the collection lens and the region accessible for scattering measurement near the bottom of the vessel.

are mounted to a carriage which translates outward with the vessel as it expands during high temperature baking. The collection optics view through a 20 cm diameter bakeable vacuum window which is protected from plasma heating and coating by a 1 cm thick quartz debris shield. A thin clam-shell shutter covers both of these elements during boronization and discharge cleaning of the vacuum vessel.

Eight of the 12 fiber optic bundles are selected to transport the light to interference filter polychromators which have been optimized for low  $T_e$  measurements. Typical transmission characteristics of the 5 channel polychromator are shown in Fig. 2. Further information about the polychromator design can be found in Ref. 4. The critical feature of the polychromator that permits low-temperature capability is the narrow bandwidth (1.6 nm) interference filter close to the laser wavelength. This filter is placed last in the polychromator cascade and a modified mount is used so that incident light can strike it normally instead of at  $4^\circ$ . This helps to reduce the bandwidth and improves out-of-band rejection. Rejection of the laser line (1064.3 nm) is about  $10^{-4}$  for this filter and is  $> 10^{-5}$  for the filters further away from the laser line.

The detectors are silicon avalanche photo diodes (RCA C30956E) with an internal gain of about 100. They are used in an electronic circuit<sup>5</sup> which provides a pulsed channel output where the background light is subtracted with a delay line technique.<sup>6</sup> This allows the full range of the 11-bit gated integrator (LeCroy 4300 FERA) to be utilized for the Thomson scattered signal. A d.c.-coupled channel provides background light measurements so that error bars based on photon statistics can be estimated accurately. The d.c. channel also permits calibration using standard d.c. light sources.

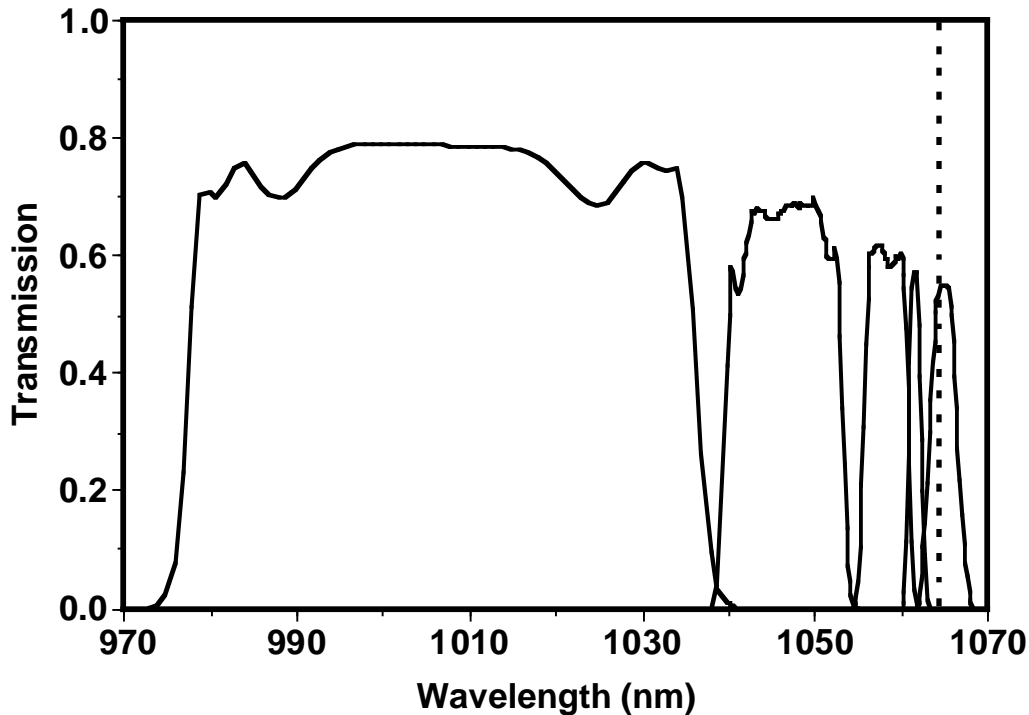


Fig. 2. Transmission of a 5 channel interference polychromator optimized for low temperature measurements.

In an effort to mitigate the expected high background light levels, carbon tiles on the floor of the vessel were recessed slightly to minimize the plasma-wall interaction in this region. High heat fluxes in the divertor precluded using razor blade viewing dumps.

The divertor region also presented access difficulties which prevented the use of a retractable laser beam alignment target. Instead, we rely on a careful initial alignment when the machine was vented and targets could be placed in the vessel, and on *in situ* alignment monitors<sup>7</sup> which indicate the transverse alignment of each laser pulse on the collection fiber optics. The alignment monitors consist of an array of five in-line 400  $\mu\text{m}$  diameter fiber optics, mounted in the focal plane of the collection optics along with the normal fibers used for the Thomson scattered signal. An avalanche photo diode detector is located at the end of each fiber so that a

crude measurement of the laser beam profile is made. The position of the peak of the profile relative to the central fiber optic is an indicator of the alignment. Typical alignment data taken during a plasma discharge is shown in Fig. 3.

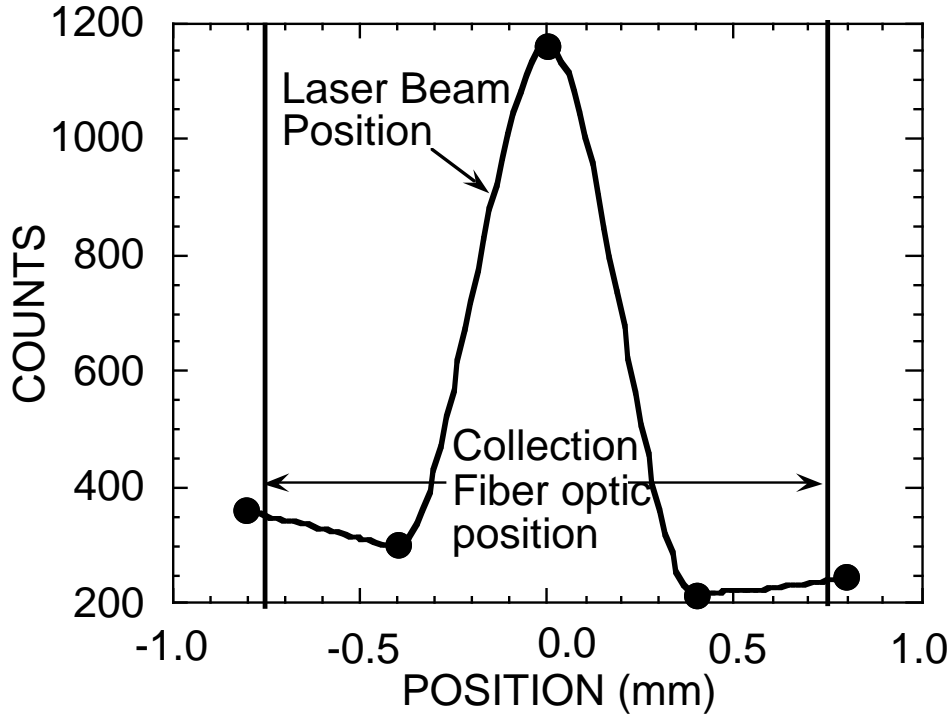


Fig. 3. Signals from an *in-situ* alignment monitor which shows the image of the laser beam on a 5 channel fiber optic array. The central region corresponds to the area viewed by the fiber optic bundle used for the Thomson scattering measurements. The peak of the signal is well centered indicating good alignment. An alignment signal is recorded for each laser pulse.



## II. TESTING AND CALIBRATION

Each detector, together with its electronics, is individually calibrated for gain and noise level in a separate test stand using both pulsed (10 ns) and d.c. light from calibrated light emitting diodes at 1060 nm. Relative channel-to-channel response of the polychromator is obtained using a computer controlled monochromator to illuminate the fiber optic input of each polychromator. The output of the monochromator is monitored with a calibrated detector (EG&G 690) traceable to NBS standards. The wavelength calibration of the monochromator is checked with an argon lamp and light from the Nd:YAG laser. This insures accurate wavelength calibration (0.1 nm) in the vicinity of the laser line which is important for low  $T_e$  measurements.

Absolute system gain was calibrated using Rayleigh scattering in argon. A typical plot of signal versus pressure is shown in Fig. 4. In spite of a sizable effort to reduce laser stray light,<sup>3</sup> several channels which view the divertor floor region near the laser entrance (channels 1-4), suffered from high stray light levels. These high stray light levels caused detector saturation which prevented Rayleigh calibration of these channels. However, after normalizing the Rayleigh factors of the non-saturated channels by the measured fiber optic and polychromator transmission, as well as the detector gain, it was found that these channels all had the same response. Rayleigh factors for the saturated channels were calculated assuming this constant response. Further work

to reduce the stray light levels is on going. The option of using Raman scattering in hydrogen to obtain an absolute calibration was dismissed owing to the safety considerations associated with such a large volume of hydrogen at substantial pressures (100 Torr).

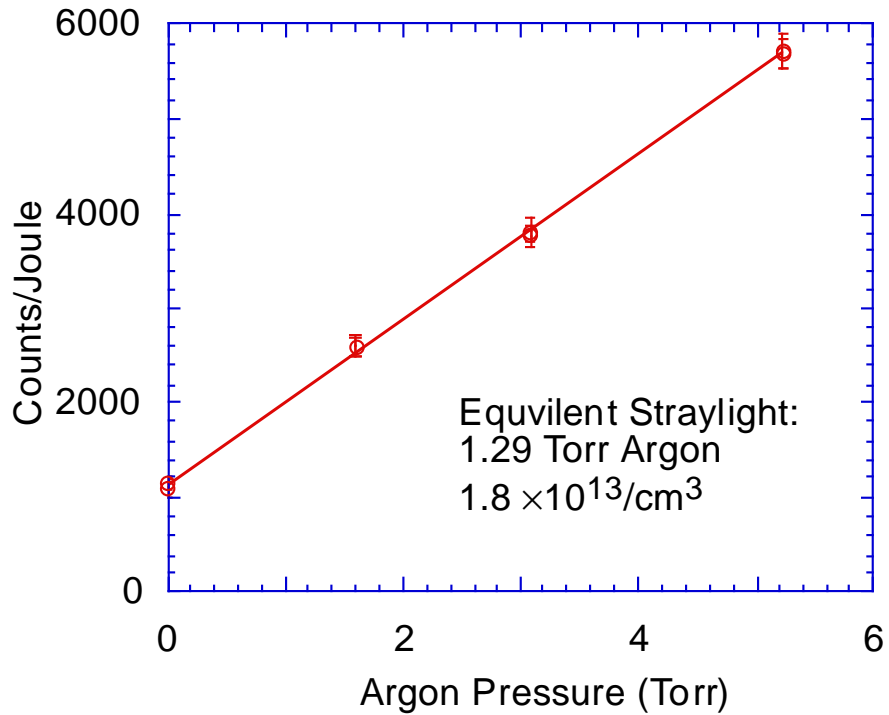


Fig. 4. Rayleigh scattering signal using argon for channel 6 at 13.8 cm above the divertor floor. The error bars represent the standard deviation of 200 laser pulses. The signal at 0 Torr represent the stray light level which, for this channel, corresponds to 1.29 Torr argon or an equivalent electron density of  $1.8 \times 10^{19} \text{ m}^{-3}$ .

### III. ANALYSIS

The measured Thomson spectrum is fitted with a least-squares fitting routine to the theoretical Thomson spectrum given by Selden,<sup>8</sup> which includes relativistic effects (important for  $T_e > 1$  keV) but not collective effects (important when the scattering parameter  $\alpha = 1/k\lambda_d \geq 1$ , *i.e.* low  $T_e$  and high  $n_e$ ). Instead of calculating the theoretical spectrum for each iteration in the fitting process, a look-up table of each wavelength channel response as a function of  $T_e$  is used. Fig. 5 graphically shows a look-up table for a typical 5 channel polychromator. Temperatures as low as 1 eV can be analyzed without using the laser channel which is often polluted with stray light. When stray light levels are low enough that the laser channel is not saturated, it can also be used in the analysis. After accounting for the portion of the signal due to stray light, the laser channel has been included for some shots and  $T_e$  measurements  $< 1$  eV have been obtained with good fits and low error bars.

The low temperature capability of this system has made possible measurements where the scattering parameter  $\alpha = 1/k\lambda_d$  is approaching 1, and collective effects begin to appear in the scattered spectrum. The highest  $\alpha$  measured to date is about 0.5, corresponding to  $T_e = 1$  eV and  $n_e = 8 \times 10^{20} \text{ m}^{-3}$ . Modeling of our system has shown that for  $\alpha < 0.8$ , only about a 20% error is made by neglecting collective effects when fitting the data. For  $\alpha > 0.8$ , a 2-dimensional minimum  $\chi^2$  fit to a model

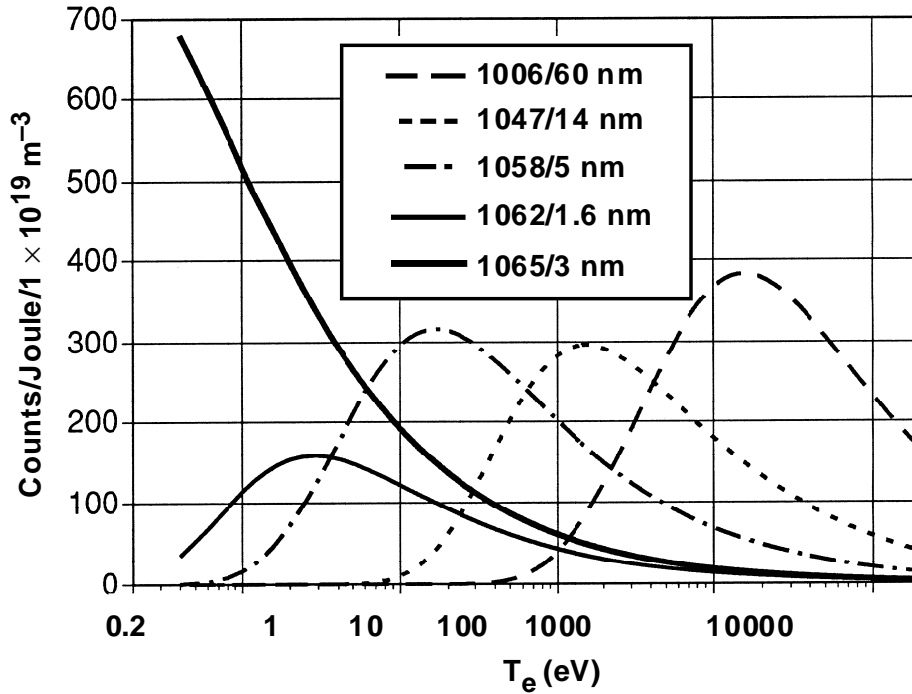


Fig. 5. Normalized detector counts versus  $T_e$  for different polychromator channels which are used in a look-up-table for a least-squares fitting routine.

which includes collective effects, such as that given by Salpeter,<sup>9</sup> is required. In the present configuration, detector saturation usually prevents measurements with  $\alpha > 0.8$ . This condition could be alleviated by reducing the detector gain or attenuating the light level with apertures. The observations of scattered spectrum with  $\alpha$  near 1, suggests the future possibility of extracting ion temperature and  $Z_{eff}$  information from these spectra by using a high dispersion resolving instrument such as a Fabry-Perot.

In order to check for systematic errors, we can compare how well the measured spectrum is represented by the theoretical Thomson spectrum. A measure of the fit is represented by the reduced chi-squared,  $\chi^2_v$ , of the least-squares fit. Because of the statistical nature of the generation of photoelectrons in the detector, we expect that for many fits, the

distribution of  $\chi_v^2$  will have a particular theoretical distribution.<sup>10</sup> The  $\chi_v^2$  probability density for a four-detector polychromator (laser channel excluded) is shown in Fig. 6. The close agreement with the theoretical curve for two degrees of freedom indicates the analytical model is consistent with the measurements, the estimated errors are appropriate, and systematic errors are insignificant.

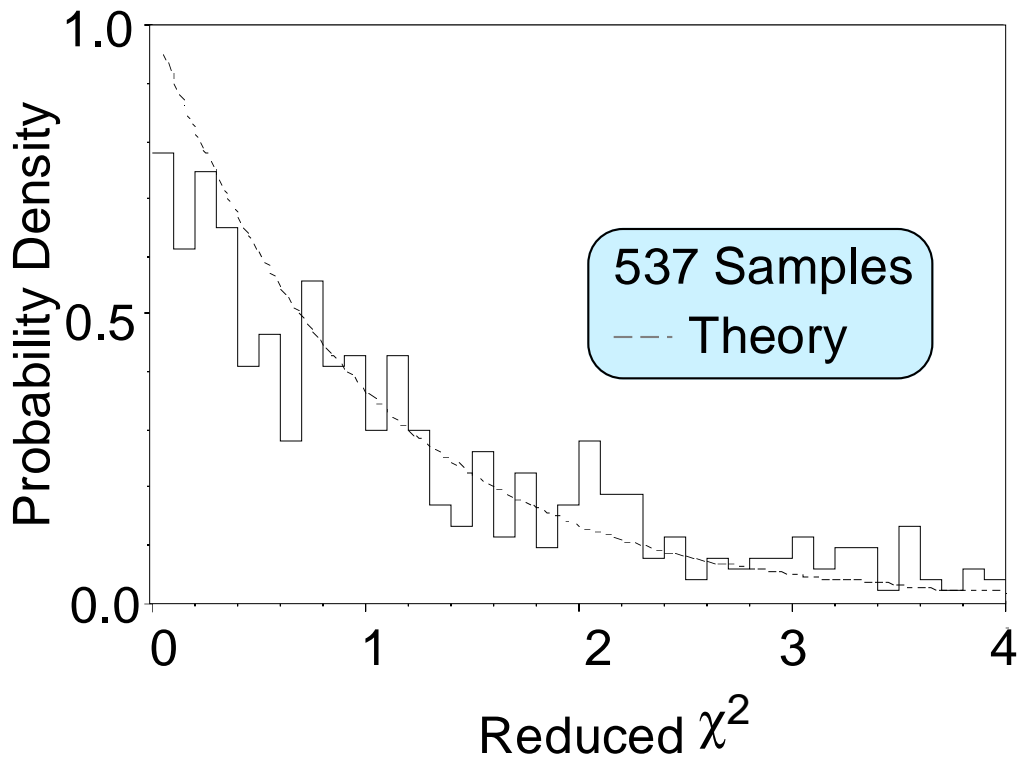


Fig. 6. Reduced  $\chi^2$  probability density for a four-detector polychromator. The data from 8 plasma discharges, totaling 473 laser pulses, is shown. The close agreement with the theoretical curve for two degrees of freedom indicates the estimated errors are consistent with the analysis model and systematic errors are insignificant.



## IV. RESULTS

The time evolution of  $T_e$  and  $n_e$  at three different locations in the divertor showing changing divertor conditions during gas puffing are shown in Fig. 7. The measurement at  $z = -116$  cm is located inside the last-closed-flux-surface, LCFS, near the edge of the main plasma as shown in the insert of Fig. 8. The measurement at  $z = -125$  cm is in the scrape-off-layer, SOL, near the X-point, and the measurement at  $z = -133$  cm is located in the private flux region. The reconstruction of the magnetic equilibrium is done with the code EFIT,<sup>11</sup> which typically determines the LCFS position to  $\pm 0.5$  cm. However, near the X-point, the accuracy is estimated to be a few cm. The determination of where the outer divertor leg intersects the floor is estimated to be  $\pm 1$  cm.

When the gas puff is turned on,  $T_e$  in the private flux region decreases and  $n_e$  increases. At about 2750 ms, there is a sharp increase in  $n_e$  in the SOL and private regions but not inside the LCFS. This is indicative of plasma detachment and MARFE formation. Several of the  $T_e$  and  $n_e$  spikes are associated with the occurrence of an ELM during the laser firing time.

Spatial profiles of divertor  $T_e$  and  $n_e$  taken along the laser path are shown in Fig. 8 at three different times for the discharge shown in Fig. 7. The high densities in the private flux region are accompanied by temperatures in the 1 eV range. Normally, the main contribution to the

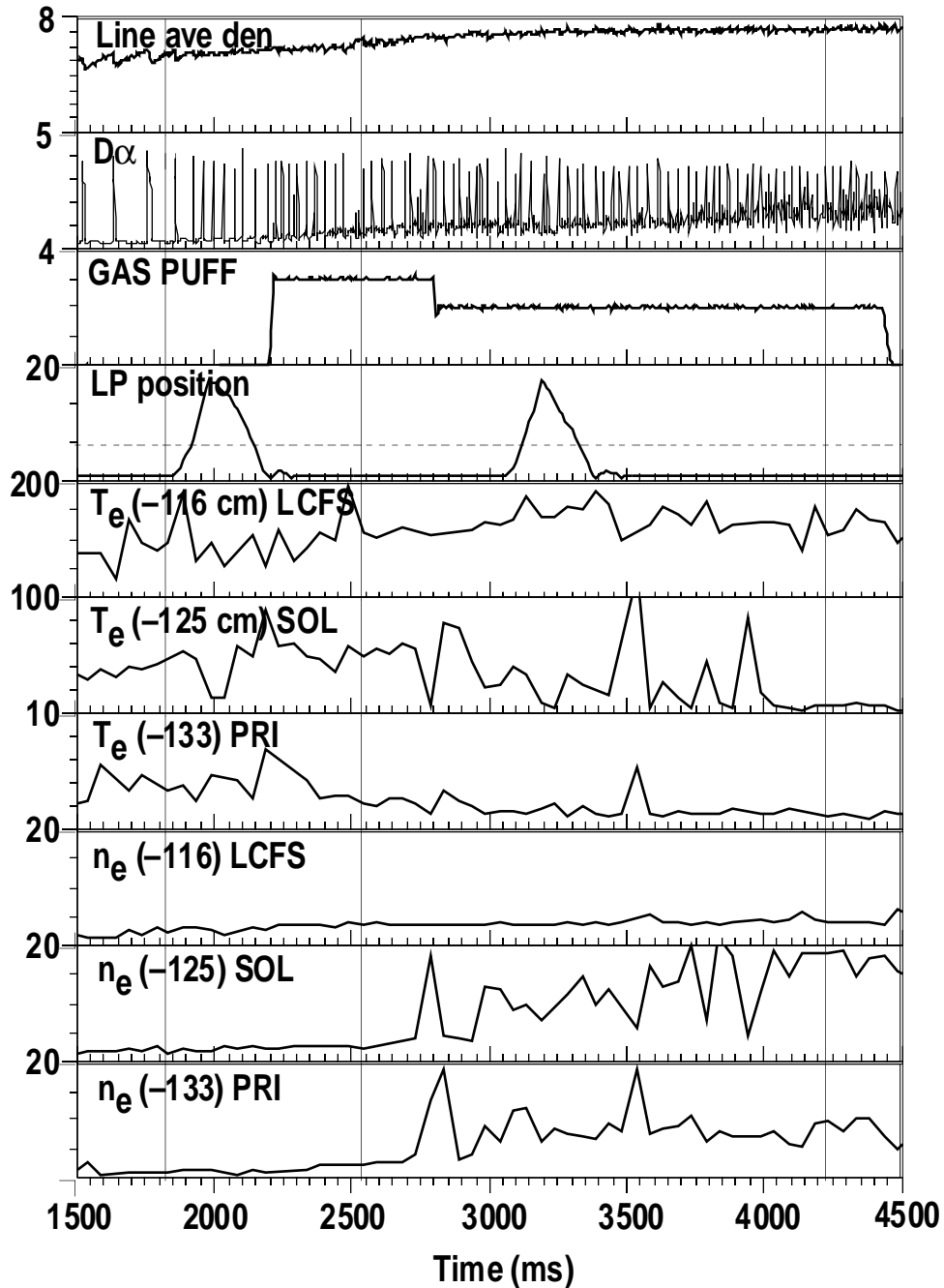


Fig. 7. Time evolution of  $\bar{n}_e$ , divertor  $D_{\alpha}$ , and  $D_2$  gas injection rate and the reciprocating Langmuir probe (LP) position above the divertor floor, together with  $T_e$  and  $n_e$  at three different locations in the divertor showing changing divertor conditions during gas puffing. The insert of Fig. 8 shows the spatial location of the measurements relative to the flux surfaces. Plasma parameters were: shot 87487,  $I_p = 1.4$  MA,  $B_T = 2.1$  T,  $P_{NBI} = 3.5$  MW, lower single null divertor, ELMing H-mode. The vertical lines indicate the times of the profiles shown in Fig. 8.

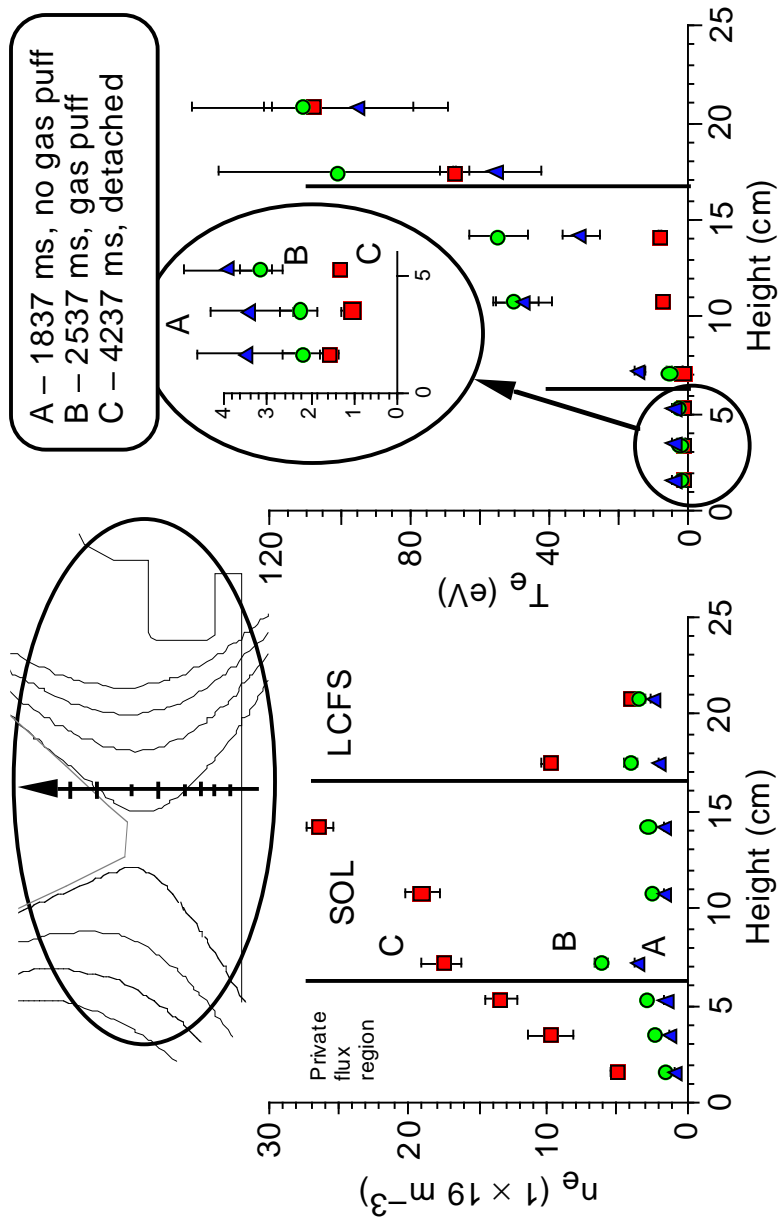


Fig. 8. Spatial profiles of divertor  $T_e$  and  $n_e$  taken along the laser path (shown in the insert) at three different times for the discharge shown in Fig. 7; (a) no gas puffing, (b) during a  $D_2$  gas puff, (c) during  $D_2$  gas puff with a MARFE formation. The low  $T_e$  results are shown in an expanded scale. The error bars represent the  $1 \sigma$  statistical uncertainty in the measurement.

error bars, which represent the  $1\sigma$  statistical uncertainty in the measurement, is predominately due to the effects of the plasma background light. At sufficiently low temperatures, the Thomson signal is present only in the 2 spectral channels near the laser line. Because these channels have narrow bandwidths, the background light is not a serious problem and the error bars are dominated by the photoelectron statistics of the Thomson scattered signal. Typical background light levels are in the range of  $(2-500) \times 10^{10}$  photons/s/nm/ $n_e^2$ /steradian, which corresponds to 10–2000 counts. Digitizer saturation occurs at 2048 counts and saturated channels are excluded from the analysis.

Two-dimensional mapping of  $T_e$  and  $n_e$  in the divertor region can be obtained by radially sweeping the X-point through the laser beam path during a steady discharge. Plots of  $T_e$ ,  $n_e$ , and  $P_e$  constructed in this way are shown in Fig. 9. Using this technique, a large portion of the divertor region can be examined to study the structure of detached and radiative divertor configurations. In the partially detached L-mode shown in Fig. 9, high density is observed in the region from the floor to the X-point. This high density region is not located at the separatrix but forms a few cm just beyond it in the SOL. Low  $T_e$  in the range of 1–3 eV accompany this high density region with higher temperatures observed in the SOL outside the X-point region. The electron pressure is highest near the X-point and drops significantly toward the separatrix and the divertor floor. These data can be used to compare the results of predictive modeling codes such as UEDGE.<sup>12</sup>

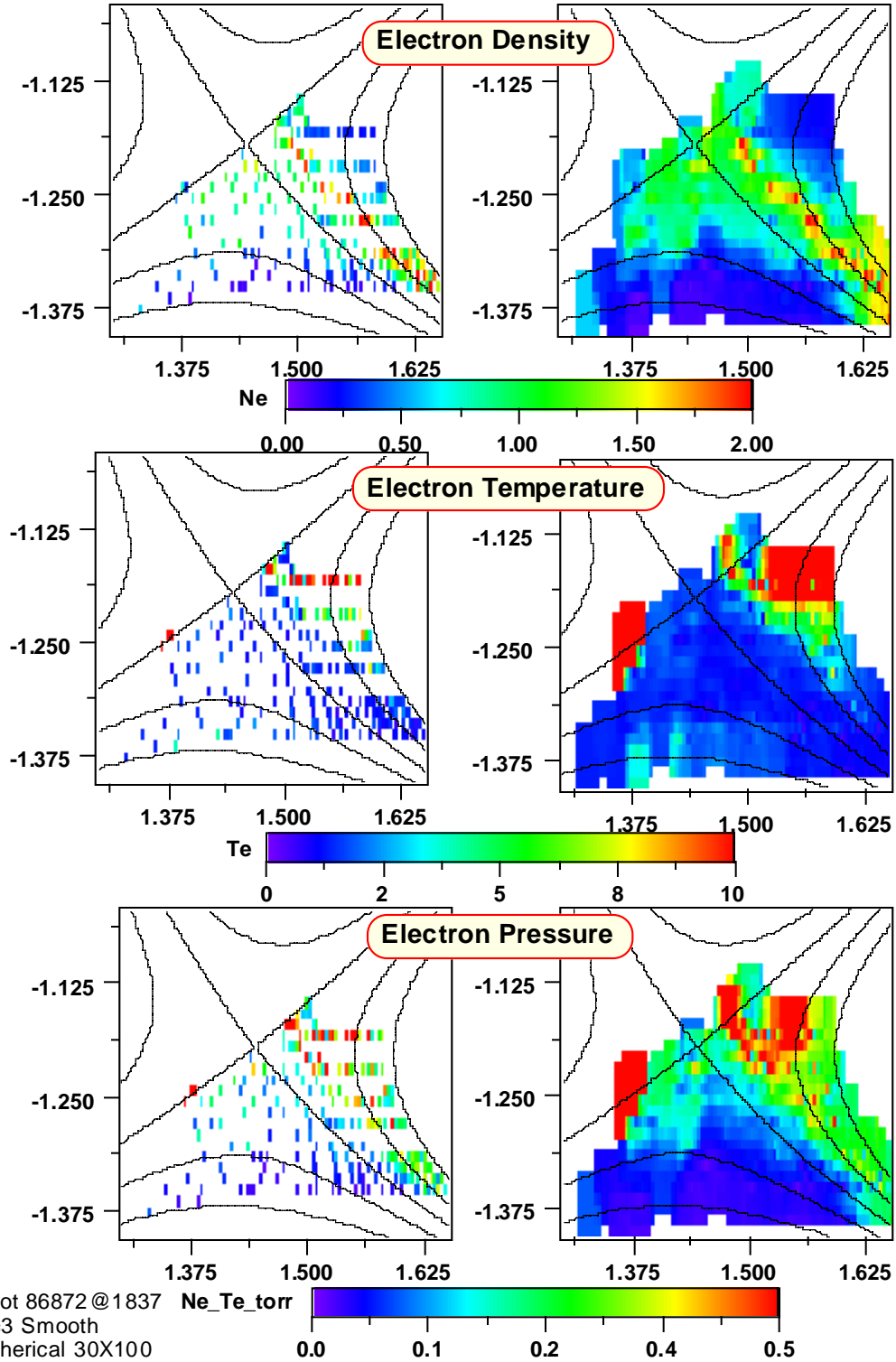


Fig. 9. 2D plot of the divertor  $T_e$ ,  $n_e$ , and  $P_e$  constructed from 13 laser pulses as the X-point was swept radially through the laser beam path. The discharge conditions were: shot 86872,  $I_p = 1.0$  MA,  $B_T = 2.1$  T,  $P_{NBI} = 1.1$  MW, lower single null divertor, partially detached L-mode. The left side of the figure shows the location of the measurements when mapped to flux coordinates. The right side of the figure shows the data smoothed so that a continuous picture is formed.

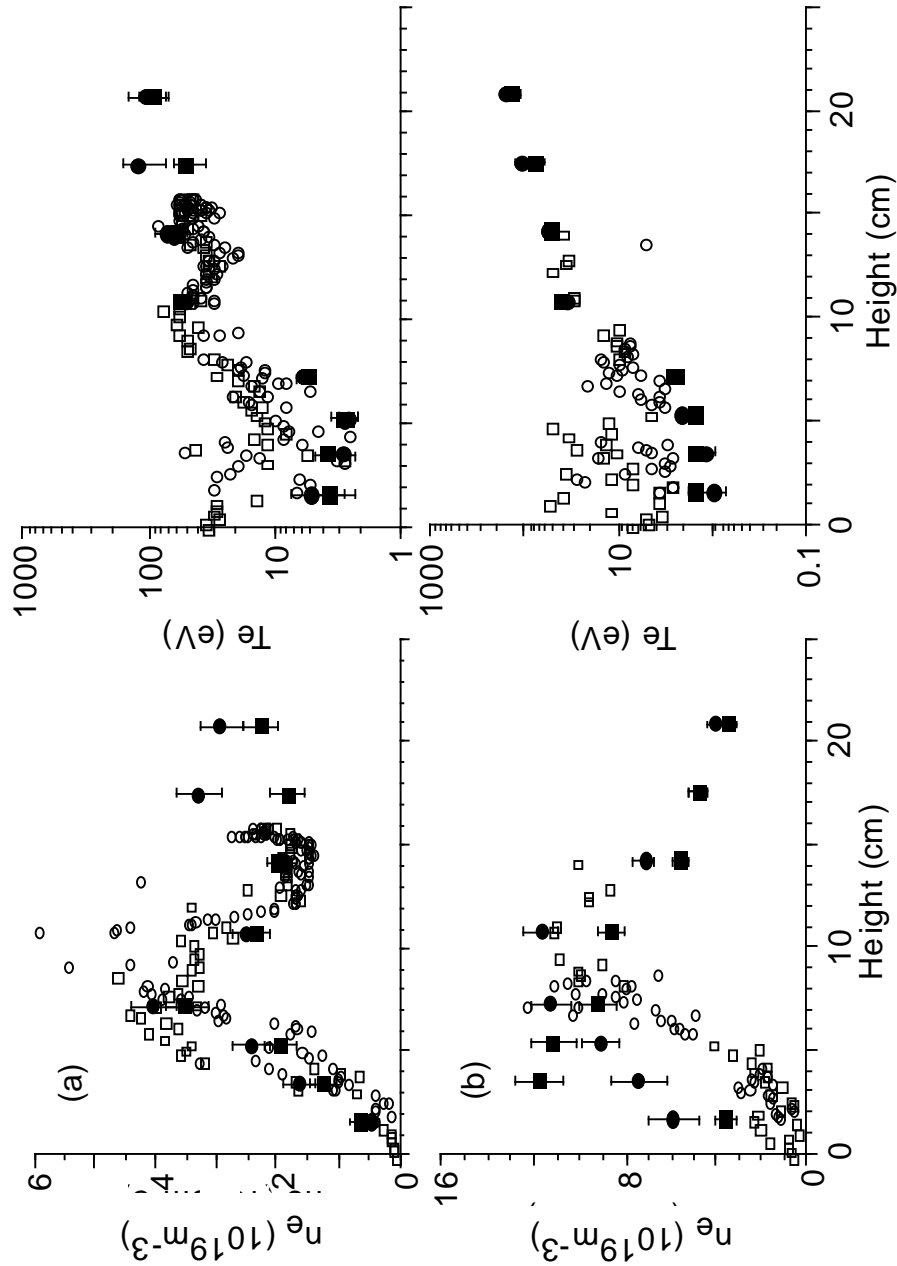


Fig. 10. Comparison of Divertor Thomson Scattering results with reciprocating Langmuir probe data for the discharge shown in Fig. 7. (a) Before gas puff at 1979 ms, (b) after gas puff at 3182 ms. The large points are from DTS and the small points are from the probe. The square points were taken during the probe insertion and the circles during the probe extraction. The DTS data were taken just before the probe insertion and just after its extraction.

A new reciprocating Langmuir probe has recently been added to the divertor region on DIII-D.<sup>13</sup> This probe measures  $n_e$  and  $T_e$  in the divertor region at the same major radius as the DTS system but at a different toroidal location. Two probe plunges were made at 1979 ms and 3182 ms for the discharge shown in Fig. 7. The effect of the probe plunge on the DTS measurements can be seen by the reduction of  $T_e(-125\text{ cm})$  at these times. Other DTS channels do not show a reduction in  $T_e$ . It is believed that the shadow of the probe only propagates to the DTS location when the field lines are predominately toroidal. This condition exists only near the X-point location.

Comparisons of DTS results with Langmuir probe measurements are shown in Fig. 10. At 1979 ms, before the D<sub>2</sub> gas puff, there is generally good agreement with DTS measured  $n_e$  slightly higher and  $T_e$  lower near the divertor floor. The high spatial resolution of the probes shows significant structure in the SOL region between the private flux region and the separatrix. After the D<sub>2</sub> gas puff at 3182 ms, there are significant differences between the two measurements. DTS measures higher  $n_e$  and lower  $T_e$  in the private flux region near the floor. Above this region the agreement is somewhat better on average. Understanding the nature and causes of these discrepancies is currently an area of active research.



## REFERENCES

- <sup>1</sup>T.N. Carlstrom *et al.*, Rev. Sci. Instrum. **63** 4901 (1992).
- <sup>2</sup>T.N. Carlstrom *et al.*, Rev. Sci. Instrum. **66** 493 (1994).
- <sup>3</sup>D.G. Nilson *et al.*, to be published in Rev. Sci. Instrum. (1996).
- <sup>4</sup>T.N. Carlstrom *et al.*, Rev. Sci. Instrum. **61** 2858 (1990).
- <sup>5</sup>C.L. Hsieh *et al.*, Rev. Sci. Instrum. **61** 2855 (1990).
- <sup>6</sup>A. Bregni and L. Giudicotti, J. Phys. E **15**, 1310 (1982).
- <sup>7</sup>P.K. Trost *et al.*, Rev. Sci. Instrum. **61** 2864 (1990).
- <sup>8</sup>A.C. Selden, Phys. Lett. A **79**, 6 (1980).
- <sup>9</sup>E.E. Salpeter, Phys. Rev. **120** 1528 (1960).
- <sup>10</sup>P.R. Bevington, *Data Reduction and Error Analysis for the Physical Sciences* (McGraw-Hill, New York, 1969).
- <sup>11</sup>L.L. Lao, *et al.*, Nucl. Fusion **25**, 1611 (1985).
- <sup>12</sup>G. Porter, "Simulations of experimentally achieved detached plasmas using the UEDGE code", to be published in Plasma Physics, 1996.
- <sup>13</sup>J.G. Watkins *et al.*, "A fast reciprocating Langmuir probe for the DIII-D divertor", this conference.



## **ACKNOWLEDGMENTS**

We wish to thank C. Makariou for electronics design and implementation, R. Ellis, D. Behne, G. Holtz, and G. Rolens for technical support, and J.C. DeBoo, R.D. Stambaugh, and S.L. Allen for program support. We also thank Jon Watkins of Sandia National Laboratories for providing Langmuir probe data. This work was supported by the U.S. Department of Energy under Contract No. DE-AC03-89ER51114.